ACADÉMIE
DES SCIENCES
INSTITUT DE FRANCE

Comptes Rendus
Physique

S. Hüller, J. D. T. Ludwig, H. A. Rose, C. Bruulsema, W. Farmer, P. Michel, A. L. Milder, G. F. Swadling and W. Rozmus

Modeling and simulations of hydrodynamic shocks in a plasma flowing across randomized ICF scale laser beams

Volume 25 (2024), p. 353-365

Online since: 22 November 2024

https://doi.org/10.5802/crphys.200

The Comptes Rendus. Physique *are a member of the Mersenne Center for open scientific publishing*
www.centre-mersenne.org — e-ISSN : 1878-1535

ACADÉMIE DES SCIENCES
INSTITUT DE FRANCE

Comptes Rendus. Physique
2024, Vol. 25, p. 353-365
https://doi.org/10.5802/crphys.200

Research article / *Article de recherche*

Modeling and simulations of hydrodynamic shocks in a plasma flowing across randomized ICF scale laser beams

Modélisation et simulations numériques de chocs hydrodynamiques dans un plasma avec flot à travers de faisceaux laser issus du lissage optique

S. Hüller[*,a], **J. D. T. Ludwig**[b], **H. A. Rose**[†,c], **C. Bruulsema**[b], **W. Farmer**[b], **P. Michel**[b], **A. L. Milder**[d], **G. F. Swadling**[b] **and W. Rozmus**[d]

[a] Centre de Physique Théorique CPHT, CNRS UMR 7644, Ecole polytechnique, Insitut Polytechnique Paris, 91128 Palaiseau Cedex, France

[b] Lawrence Livermore National Laboratory, 7000 East Avenue, Livermore, California 94551, USA

[c] Los Alamos National Laboratory, Los Alamos, New Mexico, USA 87545

[d] Department of Physics, University of Alberta, Edmonton, Alberta, Canada T6G 2E1

E-mails: stefan.hueller@polytechnique.edu (S. Hüller), ludwig8@llnl.gov (J. Ludwig), - (H. A. Rose), bruulsema1@llnl.gov (C. Bruulsema), farmer10@llnl.gov (W. Farmer), michel7@llnl.gov (P. Michel), amild@lle.rochester.edu (A. Milder), swadling1@llnl.gov (G. Swadling), wrozmus@ualberta.ca (W. Rozmus)

We wish to dedicate this article to our colleague Harvey A. Rose who passed away during our latest discussion on this work.

Abstract. High-energy laser beams interacting with flowing plasmas can produce a plasma response that leads to deflection of the beam, beam bending. Such beams have usually a speckle structure generated by optical smoothing techniques that reduce the spatial and temporal coherence in the laser field pattern. The cumulative plasma response from laser speckles slows down the velocity of the incoming flow by momentum conservation. For slightly super-sonic flow the cumulative plasma response to the ponderomotive force exerted by the beam speckle ensemble is the strongest, such that slowing down the flow to subsonic velocities leads eventually to the generation of a shock around the cross section of the beam. This scenario has been predicted theoretically and is confirmed here by our hydrodynamic simulations in two dimensions with speckled beams and in one dimension with a reduced model. The conditions of shock generation are given in terms of the ponderomotive pressure, speckle size and the flow velocity. The nonlinear properties of the shocks are analyzed using Rankine–Hugoniot relations. According to linear theory, temporally smoothed laser beams exhibit a higher threshold for shock generation. Numerical simulations with beams that are smoothed by spectral dispersion compare well with the linear theory results, diverging from those produced by beams with only a random phase plates in the nonlinear regime. The conditions necessary for shock generation and their effects on the laser plasma coupling in inertial confinement fusion (ICF) experiments are also discussed.

[*] Corresponding author

[†] Deceased

Résumé. L'interaction d'un faisceau laser de puissance avec un plasma en écoulement peut produire une réponse du plasma tel que le faisceau subit une déflection. Les faisceaux des lasers de puissance ont généralement une sous-structure de « points chauds » générée par les techniques du « lissage » optique qui a le but de réduire la cohérence spatiale et temporelle du champ laser sur la cible. La réponse cumulative du plasma chaud suite aux points chauds peut décélérer la vitesse du flot entrant due à la conservation du moment. Pour un flot faiblement super-sonique cette réponse cumulative due à la force pondéromotrice exercée par les points chauds est assez forte pour que la décélération du flot à des vitesses sub-soniques provoque la formation d'une onde de choc qui se propage contre le flot entrant. Ce scénario a été prédit par des travaux théoriques. Nos simulations hydro-dynamiques en deux dimensions avec des faisceaux « lissés » et en une dimension avec un modèle réduit confirment la formation de ce type de chocs qui dépend essentiellement du potentiel pondéromoteur des faiscaux laser, de la taille des points chauds et du nombre Mach du flot entrant. Deux méthodes de lissage optique sont étudiées, le lissage spatial par lames de phases aléatoires (random phase plates :« RPP ») et le lisssage spatio-temporel par dispersion spectrale (smoothing by spectral dispersion: « SSD »), ce dernier provoquant des chocs plus forts que dans le cas de la RPP pour le régime non linéaire des flux laser élevés. Les conditions nécessaires pour observer la formation de ce type de chocs dans le contexte de la Fusion par confinement intertiel (FCI) par laser sont également discutées.

Keywords. laser shock, laser plasma interaction, optically smoothed laser beams.

Mots-clés. chocs laser, interaction laser-plasma, lissage optique.

Funding. GENCI (allocations no. A0100500573 and AD10500573R1), US Department of Energy (contracts DE-NA0004144 and DE-AC52-07NA27344), ICF ACT-UP (subcontract no. B645970.

Manuscript received 1 May 2024, revised 9 July 2024, accepted 26 August 2024.

1. Introduction

The laser facilities designed for Inertial Confinement laser Fusion (ICF) use so-called optical "smoothing" methods for the laser beams interacting with the plasma corona in the ablating target, which is the outer target shell for the direct-drive scheme [1, 2] and the inner hohlraum wall for the indirect-drive scheme [3, 4]. Optical smoothing reduces the spatial and temporal coherence of the laser beams. It has the goal of mitigating and/or controlling the nonlinear processes related to laser-plasma interactions and hydrodynamic evolution of a target. So-called "smoothed" laser beams have a smooth intensity distribution only on a coarse scale, while on a micro-scale, in the range of the laser wavelength, they exhibit a speckle structure. Such speckles, also called laser hot spots, generally all have similar sizes, along and across the laser propagation direction, which are defined by the focusing optics, and their peak intensity follows a well-known statistical distribution.

In both direct drive and indirect drive ICF schemes, laser beams cross each other, either by design of the beam configuration or because of partial reflections from the target surface. Besides the fact that laser beams can exchange energy due to resonances with plasma waves, known as Cross Beam Energy Transfer (CBET) [5–10], such beams can have a complex substructure with important peak intensities in the speckles with values easily up to 10 times the average laser beam intensity. The ponderomotive force from the laser field on a plasma is defined as the gradient of the ponderomotive potential U. Using the definition of laser electric field $\vec{\mathscr{E}} = \frac{1}{2}[\vec{E}e^{-i\omega_0 t} + c.c.]$ with its envelope $\vec{E}$, obeying the time-dependent Helmholtz wave equation, the ponderomotive potential is defined as

$$U = e^2|\vec{E}|^2/\left(4m_e\omega_0^2\right). \tag{1}$$

where ω_0 is the laser frequency, e and m_e are the electron charge and mass, respectively. In the isothermal model of a plasma [11–13], usually satisfied for laser interactions with hot plasmas the

low-frequency plasma response can be described by the continuity and momentum equations for cold ions

$$\frac{\partial n_i}{\partial t} + \nabla \cdot (n_i \vec{v}_i) = 0 \,, \quad \frac{\partial \vec{v}_i}{\partial t} + (\vec{v}_i \cdot \nabla)\vec{v}_i = -\frac{Ze}{m_i}\nabla\phi \equiv -c_s^2 \left(\frac{\nabla U}{T_e} + \nabla \ln \frac{n_e}{n_0} \right) \tag{2}$$

where the electrostatic potential ϕ is replaced by the ponderomotive potential and the logarithm of electron density using the Boltzmann distribution for the electron density n_e, $n_e = n_0 \exp(e\phi/T_e - U/T_e)$ with n_0 describing the equilibrium density. In addition, $c_s \equiv \sqrt{ZT_e/m_i}$ stands for the ion sound speed, involving the electron temperature T_e, the ion charge Z and mass m_i. The ponderomotive potential, expressed in practical units related to the laser beam intensity, reads $\overline{U}/T_e \equiv 0.09\ (\langle I \rangle / 10^{15} \mathrm{W\,cm^{-2}})\ (\lambda/\mu\mathrm{m})^2/(T_e/\mathrm{keV})$, wherein $\langle I \rangle$ denotes the average intensity and λ stands for the laser wavelength.

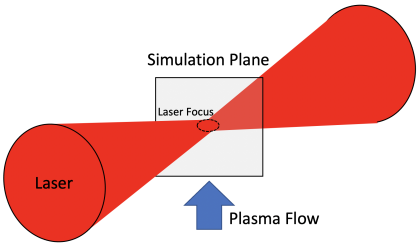

Figure 1. Schematic view of the interaction geometry: a large scale smoothed laser beam generates an imprint on the plasma in the beam focal region via its ponderomotive force. In numerical simulations, a two-dimensional (2D) domain is considered in the plane of the laser beam cross section at best focus where a super-sonic plasma flow is in the vertical direction (see the arrow).

In a flowing plasma, the process of beam bending in the direction of the flow velocity has been examined in theory and experiments [14–17]. The density perturbations resulting from the ponderomotive force of the laser are skewed by flow, which redirects the laser beam and by momentum conservation introduces a drag on the plasma flow slowing it down. The effect of beam bending is maximized producing the largest drag on the plasma flow when the flow velocity is close to the sound speed. The latter results in deceleration of the flow, and as the flow transitions from supersonic to subsonic velocity, conditions favourable to shock generation in the plasma can be reached. Our paper focuses on the formation of such shocks related to ponderomotively-driven density and velocity perturbations across the laser beam cross section. Also spatio-temporal smoothing techniques, such as smoothing by spectral dispersion (SSD), commonly used at ICF facilities can lead to shock formation, as shown in this paper. Application of the SSD and RPP beams produces an enhancement of threshold conditions for shock generation.

One can estimate that a small change in the laser field averaged momentum flux due to angular deflection of the beam, characterized by the wave vector ratio, $k_\perp/k_0$, will affect the momentum of the flowing plasma. The change of the field momentum as $(k_\perp/k_0)\langle I \rangle/c$, with $\langle I \rangle = c\epsilon_0 \langle E^2 \rangle/2$ denoting the laser intensity, has to be compared with the change in the ion momentum flux $n_i m_i c_s^2 \delta M$ were the flow reduction is normalized to the speed of sound δM. Close to sonic flow with $v_i \approx c_s$, this yields an effective reduction of the flow velocity, namely $\delta M = (k_\perp/k_0)(\langle I \rangle/5 \times 10^{14} W/cm^2)(10^{20} cm^{-3}/n_i)(1keV/T_e)$. Deflecting the beam by an angle comparable with its angular aperture $k_\perp/k_0 \sim 1/(2F)$, corresponds to a flow reduction δM of ~ 0.125 for $\langle I \rangle \approx 10^{15} W/cm^2$, $n_i = 10^{20} cm^{-3}$, the beam optical f-number $F = 8$ and for the electron temperature $T_e = 1keV$.

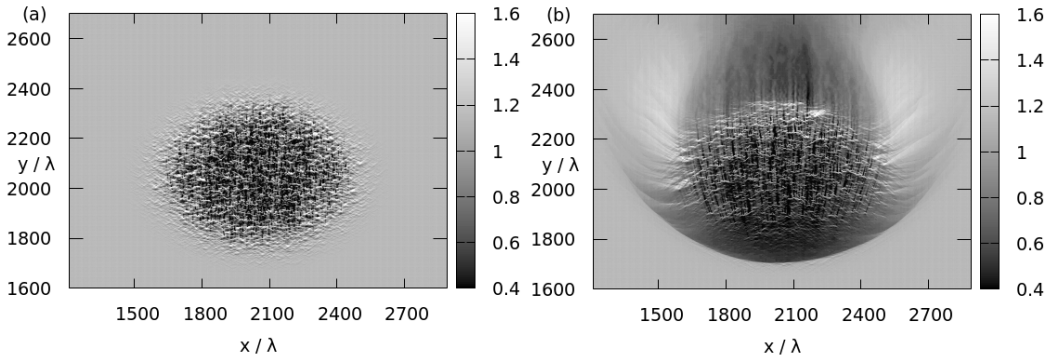

Figure 2. Cross sections from a simulation showing the plasma flow v_y/c_s (see bar with gray scale)in x and y, in units of the laser wave length λ. (a) at early time t =$40\lambda/c_s$, showing laser speckle imprint. (b) late time, t =$400\lambda/c_s$, with already developed shock front departing from the laser speckle pattern. Simulation parameters: incoming flow at M =1.2 (from below), normalized ponderomotive potential $\overline{U}/T_e$ =0.02, average electron- to critical density n_e/n_c =0.1, optical F-number F=6.

The article is organized as follows: in Section 2 the theory of laser beam deflection and shock formation in the presence of transverse flow to the beam propagation direction is summarized; in Section 3, we show the results from two-dimensional (2D) fluid simulations in which the plasma is under the influence of the ponderomotive force of an optically smoothed laser beam with speckle structure; in Section 4 we compare these 2D results with simulations, in 1D, based on the simplified model based on the drag term, as developed in Section 2; Section 5 includes conclusions and final discussions.

2. Theory of laser beam deflection and shock formation by transverse plasma flow

The collective action of the speckles in the fine structure of smoothed laser beams with their intensities up to 10× the average beam intensity can exert strong ponderomotive forces on the plasma, as described by Eq. (2). Although local flow perturbations on the scale of individual speckles may be small, their cumulative effect over large beams as used in ICF studies will lead to shock formation [18–20], which can be intensified in regions of intersecting beams.

We investigate here how the small deflection of the electromagnetic momentum flux associated with beam bending induces an opposing change in momentum by decelerating the plasma flow.

For the plasma fluid momentum $n\vec{v}_\perp$ in the direction perpendicular to the laser propagation, we consider a perturbative approach to the isothermal fluid equations (2). Linearization around the background flow velocity, $\vec{v}_0$ in the x - y plane, $\vec{v}_\perp = \vec{v}_0 + \delta\vec{v}_\perp$ leads to the following set of equations [15]

$$(\partial_t + \vec{v}_0\cdot\nabla_\perp)\ln\frac{n_e}{n_0} + \nabla_\perp\cdot\delta\vec{v}_\perp = 0, \quad (\partial_t + \vec{v}_0\cdot\nabla_\perp)\delta\vec{v}_\perp + 2\hat{\nu}_{ia}\delta\vec{v}_\perp = -c_s^2\nabla_\perp\left(\ln\frac{n_e}{n_0} + \left(1+\hat{g}\right)\frac{U}{T_e}\right) \quad (3)$$

where $\hat{\nu}_{ia}$ is a spatial convolution operator approximating Landau damping of ion acoustic perturbations. In Eq. (3) the coupling between the laser and the plasma fluid is augmented with respect to Eq. (2), by applying an additional wave-number dependent spatial convolution operator $\hat{g}$ to the ponderomotive term, that accounts for both classical and non-local heat transport effects. This correction is obtained from a closure of the energy equation, see Ref. [21] and references therein. Eq. (3) has to be solved by applying $\hat{g}$ in a Fourier space especially in

the case when thermal effects dominate ponderomotive coupling. The Fourier transformed $\widehat{g}$ reads [21] $g(k) = (1+50k\lambda_e)m_e\nu_{ei}^2/(7T_e k^2)$, where $k\lambda_e \propto T_e^2$ is the electron mean free path and $\nu_{ei} \propto T_e^{-3/2}$ is the electron-ion collision frequency. In the regime of classical thermal transport, $50k\lambda_e < 1$, the coefficient $g(k)$ scales with temperature as $g(k) \sim T_e^{-4}$; in the non-local, kinetic regime, $50k\lambda_e > 1$, it scales as $g(k) \propto T_e^{-2}$ where the spatial scale of the temperature inhomogeneity $1/k$ corresponds to $k \sim \pi/(F\lambda)$.

For the isothermal case, ignoring the correction $\widehat{g}$, a stationary equilibrium can be reached in absence of flow by balancing the local density and the ponderomotive potential, namely $(n_e/n_0)_{v_\perp=0} \equiv \exp(-U/T_e)$.

Flow can considerably modify the response of the plasma fluid [14, 15, 22–24]. Note that in the following we distinguish between the notation for local flow Mach number $\mathscr{M}$ and the incoming flow Mach number M.

The time independent solution of Eq. (3) yields in Fourier space [15]

$$[\ln n_e/n_0]_{k_\perp} = \left[\ln(n_e/n_0)_{v_\perp=0}\right]_{k_\perp}\left[1-(k_y/k_\perp)\mathscr{M}\left(k_y\mathscr{M}/k_\perp - 2i\widehat{\nu}\right)\right]^{-1}$$

in which the background flow $\vec{v}_0$ is chosen along the y-axis, the (local) Mach number $\mathscr{M} = v_y/c_s$ and the normalized damping operator $\widehat{\nu} = \nu_{ia}/(kc_s)$. The density perturbation shows a skewed profile due to the flow compared to ρ_0 in the stationary plasma and the ponderomotive potential U of a single laser speckle. This asymmetry in density perturbations averaged over speckles of the randomized laser beam leads to beam bending. In the small angle approximation the beam bending can be quantified by the averaged angular deflection rate [15] in presence of small density perturbations $\delta n = n_e - \langle n\rangle$ ($\simeq \langle n\rangle \ln(n_e/\langle n\rangle)$),

$$\frac{\partial\langle\theta\rangle}{\partial z} = \frac{\partial}{\partial z}\left\langle\frac{\vec{k}_\perp}{k_0}\right\rangle_k \cdot \vec{e}_v = -\vec{e}_v\cdot\frac{\langle\nabla_\perp\delta n\rangle_r}{2n_c} = \frac{2\beta}{F\lambda}\frac{\langle n\rangle}{n_c}\frac{\overline{U}}{T_e}\kappa\, f(\mathscr{M},\widehat{\nu}) \tag{4}$$

with $\kappa \equiv |\vec{e}_v\cdot\vec{e}_\perp|$ accounting for the projection between the unit vectors $\vec{e}_v$ and $\vec{e}_\perp$ pointing in the flow direction and the direction perpendicular to the laser propagation, respectively. Note that the averages $\langle\ldots\rangle_{k,r}$ in Eq. (4) are evaluated via integrals weighted over the squared laser field, either in the two dimensional Fourier (k)- or configuration (r)- space of any function $h(\ldots)$ namely as $\langle h\rangle_k(z) = \int|E(\vec{k}_\perp,z)|^2 h(\vec{k}_\perp)d^2k_\perp/(\int|E(\vec{k}_\perp,z)|^2 d^2k_\perp)$ and $\langle h\rangle_r(z) = \int U(\vec{x}_\perp,z)h(\vec{x}_\perp)d^2x_\perp/\overline{U}$ with the simple spatial average $\overline{U}(z) \equiv \int|E(\vec{x}_\perp,z)|^2 d^2x_\perp$. The rate of beam deflection Eq. (4) and the averaging involve the electric field amplitude $\vec{E}$ which is determined by solving the paraxial wave equation for the laser field.

The right-hand-side (rhs) of Eq. (4) has been derived in Ref. [19], see in particular Eq. (157) there, for the case of a randomized laser field generated by introducing random phase plates (RPP) in the focusing optics, which is characterized by the averaged ponderomotive potential $\overline{U}$ and the speckle correlation length, namely the effective speckle width given by $\ell_{\rm sp} = F\lambda/\beta$ with $\beta = 64/45$, and with F and λ denoting the focusing F-number and the laser wave length, respectively. The function $f(\mathscr{M},\widehat{\nu})$ in the rhs of Eq. (4), results from an integral over the angle between the flow and the wave vector of the ponderomotively driven ion acoustic waves [25]. The following expression, valid for spatially smoothed laser beams, depends on the plasma flow component across the laser beam cross section,

$$f(\mathscr{M},\widehat{\nu}) = \frac{1}{2\mathscr{M}D\sqrt{Q}}\sin\left(\psi/2\right) \quad \left(\simeq \frac{1}{2\mathscr{M}\sqrt{\mathscr{M}^2-1}} \text{ for } \mathscr{M}^2\left(1-\widehat{\nu}^2\right) > 1\right) \tag{5}$$

with the argument $\psi = \arccos([1-\mathscr{M}^2(1-2\widehat{\nu}^2)]/Q)$ as well as $Q = \sqrt{(1-\mathscr{M}^2(1-2\widehat{\nu}^2))^2 + 4\widehat{\nu}^2D^2\mathscr{M}^4}$ and $D = \sqrt{1-\widehat{\nu}^2}$ in terms of the Mach number $\mathscr{M}$, and the ion acoustic damping coefficient $\widehat{\nu}$ ($= \nu_{ia}(k)/(c_s k)$, being wave number-dependent). There is no effective beam deflection for subsonic flow, $0 \le \mathscr{M}^2 < 1$. In the close vicinity of sonic flow a resonant transfer into another

beam arises, however only over a short range until the flow is no longer orthogonal to the beam propagation. Efficient beam deflection occurs for a super-sonic flow, $\mathscr{M}^2(1-\widehat{v}^2)>1$, see Figure 3.

Note that for regimes in which thermal effects modify the laser-plasma coupling via the ponderomotive potential with the $1+\widehat{g}$ correction (see above), the rhs of Eq. (4) is modified: additional terms coming from $g(k)$ have to be taken into account via the integration over the speckle correlation function [20]. In order to determine the cumulative effect of the ponderomotive force from numerous speckles it is useful to introduce a scale separation between the mean values and the fluctuation of the fluid quantities in Eq. (3). This results [15, 20] in reduction of the averaged fluid momentum as a function of time, due to the collective action of speckles. The slowing down of the plasma flow can be described in terms of a drag force by ignoring the averages of fluctuating terms except in the last term on the rhs of Eq. (3). This leads to the set of equations

$$\partial_t\langle n\rangle+\nabla_\perp\cdot\langle n\vec{v}_\perp\rangle=0 \tag{6}$$

$$\partial_t\langle n\vec{v}_\perp\rangle+\nabla_\perp\cdot(\langle n\vec{v}_\perp\rangle\langle\vec{v}_\perp\rangle)+2\langle n\rangle\langle v_{ia}.\delta\vec{v}_\perp\rangle=-c_s^2\left(\langle\nabla_\perp n\rangle+\langle n\rangle\frac{\nabla_\perp\overline{U}}{T_e}\right)-\alpha\,\langle n\vec{v}_\perp\rangle \tag{7}$$

in which the drag coefficient α, using $\langle\delta n\nabla_\perp U\rangle_r=-\langle U\nabla_\perp\delta n\rangle_r$, for $\vec{e}_v||\vec{e}_\perp$ is given by

$$\alpha\equiv-\frac{c_s^2}{\mathscr{M}c_s}\frac{\vec{e}_v\cdot\langle U\nabla_\perp\delta n\rangle_r}{\langle n\rangle T_e}\equiv 4\beta\frac{c_s}{F\lambda}\left(\frac{\overline{U}}{T_e}\right)^2\frac{f(\mathscr{M},\widehat{v})}{\mathscr{M}}\,. \tag{8}$$

The system of Eqs. (6)-(7) describes a non linear fluid of an isothermal plasma. However, the response function used in the drag term relies on a derivation from linear theory.

In the following we assume an idealized laser beam whose spatial envelope is a slab, varying in the y-direction, and assume flow in positive y-direction with the (local) Mach number $\mathscr{M}\equiv\langle v_y\rangle/c_s>1$ at $y=0$. The density profile is initially unperturbed, but the ponderomotive force inside the speckle pattern acts on the plasma. The drag effect, as described above, leads to the deceleration of supersonic flow, transitioning it from the supersonic to subsonic flow regime. Assuming steady state flow in Eqs. (6)-(7), and neglecting the term without speckle structure $\sim\nabla_\perp\overline{U}$, we obtain $(\langle\vec{v}_\perp\rangle\cdot\nabla_\perp)\langle\vec{v}_\perp\rangle+c_s^2\nabla_\perp\ln\langle n/n_0\rangle+\alpha\langle\vec{v}_\perp\rangle\simeq 0$. For the isothermal case without thermal correction, and written in terms of the Mach number $\mathscr{M}$ this yields together with Eq. (4) and $\nabla_\perp\to\partial_y$,

$$\frac{d}{dy}\left(\mathscr{M}+\frac{1}{\mathscr{M}}\right)=-\frac{2\beta}{F\lambda}\left(\frac{\overline{U}}{T_e}\right)^2\frac{1}{\mathscr{M}^2\sqrt{\mathscr{M}^2-1}}\quad\text{yielding}\quad\frac{y_{sonic}}{y_p}=\frac{1}{2\beta}\int_{\mathscr{M}=1}^{M}\left(\mathscr{M}^2-1\right)^{3/2}d\mathscr{M} \tag{9}$$

which determines the position y_{sonic}, at which the incoming super-sonic flow is decelerated to sonic velocity. The integral in (9) is simply a function of the Mach number of the incoming flow M. The position y_{sonic} depends on the value of $\mathscr{M}$, and it defines the plasma penetration depth within the laser beam necessary for the onset of shock formation, see Figure 4; y_{sonic} scales with $y_p=F\lambda/(\frac{\overline{U}}{T_e})^2$, i.e. with the effective speckle width, $F\lambda/\beta$ and is inversely proportional to the square of the ponderomotive potential. For regimes in which thermal effects dominate the laser-plasma coupling, the y_{sonic} length will be modified with respect to Eq. (9).

Knowing the function $f(\mathscr{M},\widehat{v})$ for the randomised laser beam such as Eq. (5) for the RPP, the average momentum and continuity equations (7) can be solved in one spatial dimension along the flow y-direction. This results in the formation of a shock propagating against the incoming flow, due to the action of the drag force and the ponderomotive force at the edges of the spatially averaged laser beam profile. In Section 3 we will show full 2D simulations of Eq. (3) including the beam speckle structure, for which the knowledge of $f(\mathscr{M},\widehat{v})$ is not needed. We compare these results with simulations of this simplified 1D model in Section 4.

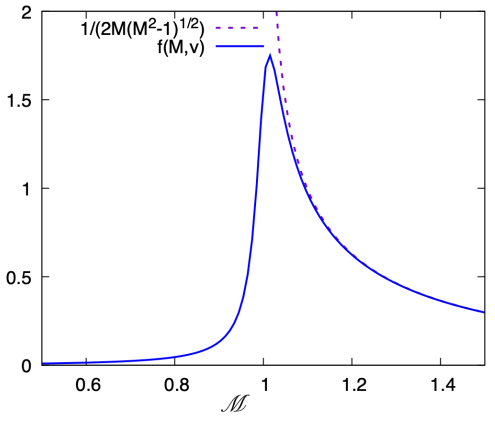

Figure 3. Plasma response from Eq. (5), $f(\mathscr{M},\hat{v}=0.025)$ as a function of the (local) flow Mach number $\mathscr{M}$. Dashed: approximation, also given in Eq. (5).

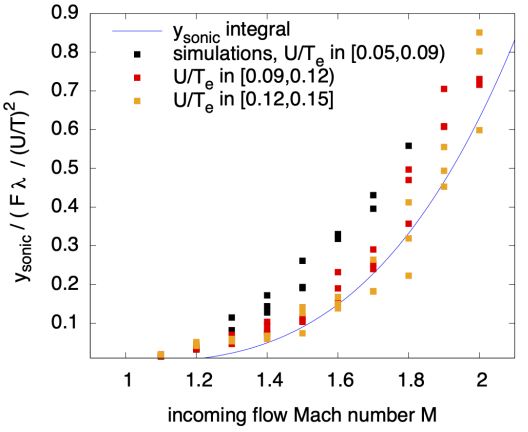

Figure 4. Scaled position y_{sonic} from Eq. (9) (line) and from RPP simulations (data points). Different colours indicate the interval of $\overline{U}/T_e$ values.

3. Shock formation in numerical simulations with optically smoothed laser beams

We have performed numerical simulations with a conservative hydrodynamic scheme, based on the Clawpack package [26, 27] and adapted to a hot isothermal plasma [28] in two dimensions (2D). The ponderomotive potential of the laser beam with speckle structure, taken in a single cross section close to the laser beam focus was applied as source term in Eq. (2). For these simulations an initially homogeneous electron density of n_e =0.1n_c is assumed where n_c is the critical density. The simulations are performed in dimensionless units, where spatial coordinates are normalized to the laser wavelength λ and time is measured in λ/c_s. The ion sound speed, c_s, reads in practical units as $\sim 0.3\mu$m/ps $\times\sqrt{ZT(keV)/A}$.

For the smoothed laser beams we have used the focusing F-number F =8. The spatial domain was resolved with 4096x4096 mesh points. For the typical laser wave length of λ =0.351μm this corresponds to a domain size defined by $L_x = L_y$ =1.977mm. The spatial incoherence of laser beams is introduced using the top hat model for the Random Phase Plates (RPP) [29]. For the beam intensity distribution within the x–y-plane inside the plasma, the corresponding near field configuration at the focusing lens is composed of elements with a random phase $\phi(\vec{k})$, i.e. 0 or $\pi/2$ (RPP), and a constant amplitude $|E(\vec{k})|$ for $|\vec{k}| \le k_0/(1+4F^2)^{1/2}$ (and 0 outside) with $k_0 = 2\pi/\lambda$ for the laser wave number. The laser electric field in the interaction zone, where the plasma is situated, is computed via the Fourier transform of $E(\vec{k}_\perp)\exp(i\,k_\perp^2\,z/2k_0)$. The cross-section of the speckle patterns produced by such disk-shaped RPP beams are seen in the ponderomotively induced flow velocity (v_y/c_s) perturbations in Figure 2, left subplot. In the same figure, right subplot, a smooth shock front emerges from the region dominated by the beam speckle pattern.

In an early stage of shock formation, the position y_{sonic} at which the flow transitions from the super- ($y < y_{sonic}$) to the sub-sonic ($y > y_{sonic}$) velocity appears inside and close to the edge of the laser beam cross section with a speckle structure. This position y_{sonic} has been determined from a set of simulations with RPP-smoothed laser beams by varying the amplitude of $\overline{U}/T_e$ and the incoming flow Mach number M. The comparison with the theory developed in the preceding section, Eq. (9), blue line, shows good agreement between simulations and the model, and confirms the scaling with $y_p = F\lambda/(\frac{\overline{U}}{T_e})^2$. Different colours distinguish data points with different ponderomotive coupling strength, see legend.

The shock front that emerges from the beam cross section, as seen in Figure 2, right subplot, can be quantified by determining the density and flow speed jumps, n_1/n_0, and v_y/c_s, respectively, as illustrated for the central cut in x in Figure 5.

At the major laser laser facilities dedicated to ICF and laser-plasma interaction experiments, spatio-temporal smoothing techniques are used, in particular Smoothing by Spectral Dispersion (SSD)[30, 31] such as at the US National Ignition Facility (NIF), the OMEGA laser at the University of Rochester and the French Laser MégaJoule (LMJ). SSD makes use of a bandwidth in the laser pulse in combination with a grating that tilts the phase front and consequently introduces phase modulation. This leads to speckle motion [32], which is in contrast to the steady state speckle pattern for the case of RPP. Both transverse and longitudinal SSD methods exist, and a combination of both. For longitudinal SSD important speckle motion arises in the direction longitudinal to the beam propagation, while for transverse SSD speckles move both in transverse and longitudinal direction [33]. We restrict ourselves here to transverse SSD, as is implemented on the NIF. The sinusoidal phase modulations to the pulse introduce bandwidth before the beam passes through a dispersion grating, which can be written in terms of the electric field at the lens, $\mathbf{E}(y,t) = \frac{1}{2}\mathbf{E}_0(y,t)\exp\{i[\omega_0 t + \delta_m \sin(\omega_m t + 2\pi N_{\rm cc} y/w_y) + \phi_0]\} + c.c.$ where ω_0 is the central laser frequency, ϕ_0 the initial phase, ω_m the modulation frequency, δ_m the modulation depth (here = 0.6), w_y is the beam width in y direction, and $N_{\rm cc}$ is called the number of colour cycles that characterizes the time delay $\Delta\tau = N_{cc}T_m$ introduced by the grating over the period of modulation, $T_m = 2\pi/\omega_m$. The resulting total bandwidth of the laser pulse $\Delta\omega \approx 2\delta_m\omega_m$ which is still small relative to the ω_0. The value of δ_m has to be multiplied by 3 for frequency-tripled laser pulses (λ =0.351μm).

In our simulations by applying the spatio-temporal smoothing technique SSD, we observe very similar evolution of the shock front departing from the laser beam cross section, as seen for the case of RPP. Please consult Ref. [25] for details that distinguish RPP and SSD as far as the y_{sonic} position is concerned. The results for SSD are in qualitative agreement with RPP simulations, as shown in Figure 6, which summarizes results from a set of simulations by varying the incoming flow Mach number M and $\overline{U}/T_e$. However, for the same parameters M and $\overline{U}/T_e$ >0.08, the effect of transverse SSD tends to produce stronger shocks with respect to RPP. Note that for transverse SSD speckle motion occurs in the beam cross section, which is not the case for the longitudinal SSD (and for which we have not carried out simulations).

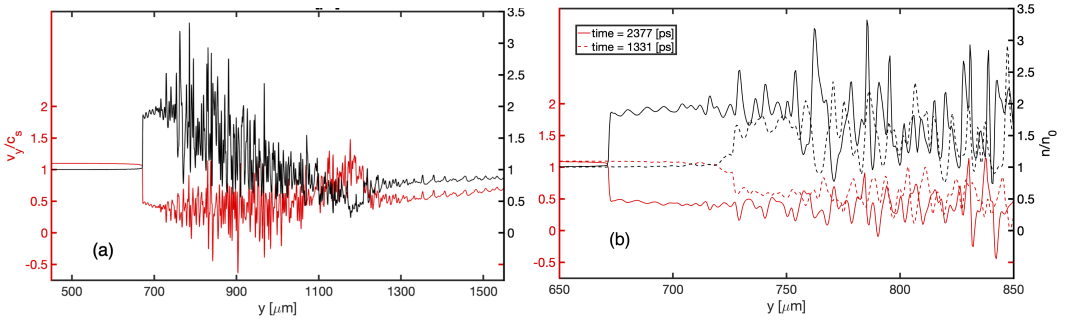

Figure 5. Density and flow profiles, n_1/n_0 (in black) and v_y/c_s (red colour), respectively, along the y-axis across the beam propagation and along the incoming supersonic flow, here M =1.2 taken in the center of the beam cross section. Left (a) : profiles across the entire laser beam speckle pattern taken at late time, t =2.38ns, right (b): profiles zoomed around the shock emerging from the speckle pattern, y ~700μm, taken at two instants, t =1.33ns and later t =2.38ns. Spatial units in μm for λ = 0.351μm. Parameters: $\overline{U}/T_e$ =0.1, n_0/n_c =0.1.

4. Shock strength and shock speed: 2D simulations vs. 1D modeling

The results of our sets of simulations are shown in Figures 6 and 7 for cases with pure spatial and with spatio-temporal smoothing, RPP and SSD, respectively, both for the shock strength in terms of the density jump across the shock front, n_1/n_0, and the shock speed in the laboratory frame $v_{\rm sh}/c_s$. Shown are the values for both the full 2D simulations with speckles in the laser beam cross section and 1D simulations in the single y-direction, solving the non linear Eqs. (6)-(7) with the drag term $\sim \alpha$ that accounts for the cumulative effect of speckles.

The computationally much less expensive 1D simulations with a drag force show good agreement with the 2D simulations with speckled laser beams. We observed the good agreement between results of two simulations in spite of the linear plasma response function (5) used in Eq. (7) to model the nonlinear physics of the shock front steepening. In particular the values obtained for the shock speed are well reproduced, while the 1D model leads to slightly stronger shock strength for M >1.1. Both sets of values are determined from the shock front evolution as shown in Figure 5 for the 2D simulations.

The speed of the emerging shock depends on the ponderomotive force and can be determined by integrating the Eqs. (6)-(7) in steady state from unperturbed plasma upstream of the shock front into the region of the speckled beam cross section. It yields for the cases of RPP (without temporal smoothing, i.e. not for SSD), the following relation between the density jump n_1/n_0, the ponderomotive potential $\overline{U}/T_e$, Mach number of the incoming flow, and the shock speed in the laboratory frame,

$$\left(\mathcal{M} - \frac{v_{\rm sh}}{c_s}\right)^2 = 2\frac{\overline{U}/T_e + \ln(n_1/n_0)}{1-(n_1/n_0)^{-2}}. \tag{10}$$

for the derivation of which we have used the continuity equation in the shock frame. The data points in Figure 7 correspond to the values directly deduced from the simulations, by inspecting the advancing shock front for each case. The lines in Figure 7 have been deduced from our model, Eq. (10), that takes into account the ponderomotive action of the laser beam on the plasma flow. For the evaluation of expression Eq. (10) we have used the values for the density jumps (reported in Figure 6) from our simulations in order to determine $-v_{\rm sh}/c_s$, as shown in the lines of Figure 7.

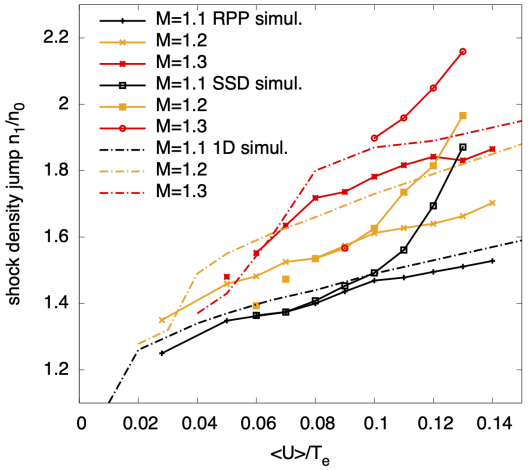

Figure 6. Shock density jump, for RPP and SSD full 2D simulations (lines with data points) and 1D simulations of Eq. (7) (dash-dotted) as a function of the normalized ponderomotive potential $\overline{U}/T_e$ for Mach number values of the incoming flow, M =1.1, 1.2, and 1.3. Beam F-number F =8.

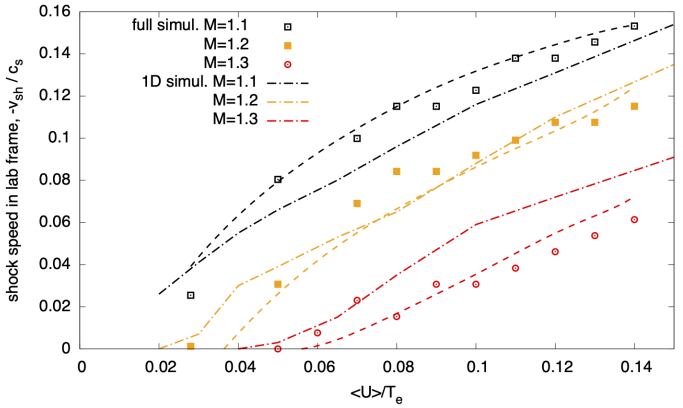

Figure 7. Speed of the shock front after outbreak from the beam cross section, from full 2D RPP simulations (data points), 1D simulations (dash-dotted), and values following Eq. (10) (dashed), as a function of $\overline{U}/T_e$ for incoming flow with M =1.1, 1.2, and 1.3.

Our simulations confirm that the values obtained for smooth shock fronts that propagate outside the beam cross section obey the Rankine–Hugoniot relations (e.g. [34]) for continuity and momentum up- and downstream of the discontinuity in the shock's reference frame. [25] For an isothermal plasma, as considered in our simulations, we disregard the internal energy relations on both sides of the shock. For this case, the sound speed is the same on both sides, such that the simplified Rankine–Hugoniot relations result in $n_1/n_0 = \mathcal{M}_0^2 = \mathcal{M}_1^{-2}$ together with $\mathcal{M}_0\mathcal{M}_1 = 1$, in the shock frame, with '0' for upstream, unperturbed, and '1' for downstream. The resulting density jump is then essentially a function of the Mach numbers, relating $\mathcal{M}_1^2 = M^2$ to the incoming flow, and to the shock speed $v_{\rm sh}$ in the laboratory frame as $-v_{sh}/c_s = \sqrt{n_1/n_0} - M$. This implies that the formation of a shock propagating against the incident flow ($-v_{sh} > 0$) can only occur for a sufficiently high density jump, namely $n_1/n_0 > M^2$; consequently for M =1.1, 1.2, and 1.3 this means that shocks should not be able to leave the laser beam cross-section and propagate freely unless n_1/n_0 >1.21, 1.44, and 1.69, respectively. This explains also why both 2D and 1D simulation data in Figure 7 for M =1.3 are incomplete for smaller $\overline{U}/T$ values. Consequently, the data points for M =1.3 and $\overline{U}/T_e$ <0.08 have large uncertainty. At the same time, as shown in Figure 6, the strength of the shock in terms of the jump conditions increases with the incoming flow Mach number M, as a consequence of the condition $n_1/n_0 > M^2$, and increases with the cumulative action of the ponderomotive force in the beam speckles, $\propto \overline{U}/T_e$.

It is important to note that the time required in simulations (in particular in 2D) to observe a shock emerging out of the laser beam cross-section can be very long, beyond the run time of our simulations, because of the low shock speed. This trend of lower shock speeds, but at the same time higher shock strengths, increases with the incoming Mach number as seen in Figure 7.

5. Conclusion

We have shown that optically smoothed laser beam with speckle structure can lead to the formation of macroscopic shocks emerging from the beam cross section in presence of incoming flow that has a supersonic speed perpendicular to the laser beam propagation axis.

It is known from earlier work [14, 15, 22–24] that plasma flow with a component orthogonal to the propagation direction of a laser beam can deflect the beam when the flow velocity is close to the sound speed of the plasma. The ponderomotive force of the beam's laser field acts on the plasma such that incoming supersonic flow is slowed down. For sufficiently strong fields the

plasma response, see Eq. (5) and Figure (3), leads to the transition form super- to subsonic flow, which gives rise to the formation of density and flow perturbations that eventually steepen and develop a shock propagating against the incoming flow direction.

For optically smoothed laser beams with speckle structure, a smooth shock front forms due to the cumulative action of the ponderomotive force from the laser speckle ensemble. The characteristic distance of plasma penetration across the randomized laser beam required for the flow to slow down to subsonic velocity and form a shock, given by Eq. (9), defines the necessary condition for the shock generation. The emergence of such shocks occurs as a result of laser beam bending and subsequent momentum change induced by the redirected laser light. Beam bending and the shock formation occur over a limited range along the beam propagation until the flow component perpendicular to the deflected beam becomes subsonic. Such scenarios are likely to occur in laser-generated hot plasmas in the context of laser-driven ICF, both for the indirect- and the direct-drive schemes. The beam bending [14–17] is an important mechanism that can alter the angular spectra of the laser beams similarly to self-focusing and stimulated scattering instabilities enhanced by the plasma waves excited by speckles in a flowing plasma. The shock formed by the beam's action on the plasma flow affects the plasma hydrodynamic evolution and can impact the propagation of neighbouring beams, eventually leading to uncontrolled beam deflection in multi-beam configurations.

Based on our simulations with RPP beams, we can estimate the energy required in experiments to observe the effect of shock formation. The scaling of Eqs. (8) and (9) predicts stronger effects for relatively small speckle sizes that can be attained by bundles of beams crossing at small angles. The latter leads to reduced effective F-numbers, characterizing the speckles in the beam cross section, with respect to the F-number of a single beam. As a realistic example, based on multi-beam configurations, we assume the effective F-number such that $F\lambda \sim 1\mu m$, the average laser intensity $I = 2 \times 10^{15}$ W/cm^2, and the electron temperature T_e=2 keV, resulting in the normalized ponderomotive potential $\overline{U}/T_e \approx 0.011$. For incoming flow Mach numbers M, corresponding to $1.05 \leq M \leq 1.2$, we find then that the estimated time to observe such a shock, would be roughly 1.3-2.7 ns. Hence, within the square cross section of 400μm$\times$ 400μm or 810μm $\times$ 810μm of the laser beam with an average intensity $I = 2 \times 10^{15}$ W/cm^2 will require the laser energy of 9kJ or 36kJ, respectively.

The set of model equations Eqs. (6)-(7) for the transverse flow, with the drag coefficient α that accounts for the cumulative action of speckles and knowing the response function $f(\mathscr{M},\hat{v})$ for the smoothing technique (see Eq. (5) for RPP, see also [25]), can potentially be implemented in radiation-hydrodynamics codes to examine the slowing down of flow, without resolving the detail of the speckle structure.

In the current work, we have restricted ourselves to the case of an isothermal plasma without any effects from local or non-local heat transport and collisional plasma heating. The latter may play a role in cases of non-uniform heating and/or transport mechanisms with electron mean free paths comparable or beyond the speckle size. This may be of importance for plasma electron temperatures below 1keV. Currently we study the shock generations taking into account such processes, both by considering the enhancement of the speckle structure and its ponderomotive force following adequate models [21] and by performing numerical simulations taking into account collisional absorption and thermal transport.

Acknowledgments

S. H. acknowledges the access granted to the French HPC resources of IDRIS under the allocations A0100500573 and AD010500573R1 by GENCI, as well as the support by the CPHT computer team. A. M. and W. R. acknowledge support from the Digital Research Alliance of Canada and support

from the U.S. Department of Energy Contract number: DE-NA0004144. This work was performed under the auspices of the U.S. Department of Energy by Lawrence Livermore National Laboratory under Contract DE-AC52-07NA27344 and by LLNL's WPD, ICF Program's Academic Collaboration Teams's University Program (ACT-UP) under Subcontract No. B645970.

Declaration of interests

The authors do not work for, advise, own shares in, or receive funds from any organization that could benefit from this article, and have declared no affiliations other than their research organizations.

References

[1] R. S. Craxton, K. S. Anderson, T. R. Boehly, et al., "Direct-drive inertial confinement fusion: A review", *Phys. Plasmas* **22** (2015), no. 11, article no. 110501.

[2] E. M. Campbell, T. C. Sangster, V. N. Goncharov, et al., "Direct-drive laser fusion: status, plans and future", *Philos. Trans. R. Soc. Lond., Ser. A* **379** (2021), no. 2189, article no. 20200011.

[3] J. Lindl, "Development of the indirect-drive approach to inertial confinement fusion and the target physics basis for ignition and gain", *Phys. Plasmas* **2** (1995), no. 11, pp. 3933–4024.

[4] O. A. Hurricane, P. K. Patel, R. Betti, et al., "Physics principles of inertial confinement fusion and U.S. program overview", *Rev. Mod. Phys.* **95** (2023), article no. 025005.

[5] W. L. Kruer, S. C. Wilks, B. B. Afeyan and R. K. Kirkwood, "Energy transfer between crossing laser beams", *Phys. Plasmas* **3** (1996), no. 1, pp. 382–385.

[6] R. K. Kirkwood, B. B. Afeyan, W. L. Kruer, et al., "Observation of Energy Transfer between Frequency-Mismatched Laser Beams in a Large-Scale Plasma", *Phys. Rev. Lett.* **76** (1996), pp. 2065–2068.

[7] V. V. Eliseev, W. Rozmus, V. T. Tikhonchuk and C. E. Capjack, "Interaction of crossed laser beams with plasmas", *Phys. Plasmas* **3** (1996), no. 6, pp. 2215–2217.

[8] P. Michel, L. Divol, E. A. Williams, et al., "Tuning the Implosion Symmetry of ICF Targets via Controlled Crossed-Beam Energy Transfer", *Phys. Rev. Lett.* **102** (2009), article no. 025004.

[9] P. Michel, L. Divol, E. A. Williams, et al., "Energy transfer between laser beams crossing in ignition hohlraums", *Phys. Plasmas* **16** (2009), no. 4, article no. 042702.

[10] A. Colaïtis, D. Hüller S.and Pesme and V. T. Duchateau G.and Tikhonchuk, "Crossed beam energy transfer: Assessment of the paraxial complex geometrical optics approach versus a time-dependent paraxial method to describe experimental results", *Phys. Plasmas* **23** (2016), no. 3, article no. 032118.

[11] J. Candy, W. Rozmus and V. T. Tikhonchuk, "Nonlinear ion waves driven by the periodic ponderomotive force", *Phys. Rev. Lett.* **65** (1990), pp. 1889–1892.

[12] S. Hüller, "Stimulated Brillouin scattering off nonlinear ion acoustic waves", *Phys. Fluids B* **3** (1991), no. 12, pp. 3317–3330.

[13] H. A. Rose, "Saturation of stimulated Brillouin scatter by self-consistent flow profile modification in laser hot spots", *Phys. Plasmas* **4** (1997), no. 2, pp. 437–446.

[14] D. E. Hinkel, E. A. Williams and C. H. Still, "Laser Beam Deflection Induced by Transverse Plasma Flow", *Phys. Rev. Lett.* **77** (1996), pp. 1298–1301.

[15] H. A. Rose, "Laser beam deflection by flow and nonlinear self-focusing", *Phys. Plasmas* **3** (1996), no. 5, pp. 1709–1727.

[16] J. D. Moody, B. J. MacGowan, D. E. Hinkel, et al., "First Optical Observation of Intensity Dependent Laser Beam Deflection in a Flowing Plasma", *Phys. Rev. Lett.* **77** (1996), pp. 1294–1297.

[17] B. Bezzerides, "Intrinsic bending of a laser beam in a flowing plasma", *Phys. Plasmas* **5** (1998), no. 7, pp. 2712–2720.

[18] H. A. Rose and S. Ghosal, "Effect of smoothing by spectral dispersion on flow induced laser beam deflection: The random phase modulation scheme", *Phys. Plasmas* **5** (1998), no. 3, pp. 775–781.

[19] S. Ghosal and H. A. Rose, "Two-dimensional plasma flow past a laser beam", *Phys. Plasmas* **4** (1997), no. 7, pp. 2376–2396.

[20] S. Ghosal and H. A. Rose, "Effect of induced spatial incoherence on flow induced laser beam deflection: Analytic theory", *Phys. Plasmas* **4** (1997), no. 12, pp. 4189–4191.

[21] H. A. Rose and D. F. DuBois, "Modification of stimulated Brillouin, saturated Raman scattering and strong Langmuir turbulence by nonlocal heat transport", *Phys. Fluids B* **4** (1992), no. 6, pp. 1394–1396.

[22] R. W. Short, R. Bingham and E. A. Williams, "Filamentation of laser light in flowing plasmas", *Phys. Fluids* **25** (1982), no. 12, pp. 2302–2303.

[23] A. J. Schmitt, "The effects of plasma flow on thermal and ponderomotive light filamentation", *Phys. Fluids B* **1** (1989), no. 6, pp. 1287–1294.

[24] C. Ruyer, P. Loiseau, G. Riazuelo, R. Riquier, A. Debayle, P. E. Masson-Laborde and O. Morice, "Accounting for speckle-scale beam bending in classical ray tracing schemes for propagating realistic pulses in indirect drive ignition conditions", *Matter Radiat. Extremes* **8** (2023), no. 2, article no. 025901.

[25] J. D. Ludwig, S. Hüller, H. A. Rose, et al., "Shock formation in flowing plasmas by temporally and spatially smoothed laser beams", *Phys. Plasmas* **31** (2024), no. 3, article no. 032103.

[26] R. J. LeVecque, "Wave Propagation Algorithms for Multidimensional Hyperbolic Systems", *J. Comput. Phys.* **131** (1997), no. 2, pp. 327–353.

[27] R. J. LeVeque, *Numerical Methods for Conservation Laws*, 2nd edition, Birkhäuser: Basel, 1992.

[28] S. Hüller, P. E. Masson-Laborde, D. Pesme, M. Casanova, F. Detering and A. Maximov, "Harmonic decomposition to describe the nonlinear evolution of stimulated Brillouin scattering", *Phys. Plasmas* **13** (2006), no. 2, article no. 022703.

[29] H. A. Rose and D. F. DuBois, "Statistical properties of hot spots produced by a random phase plate", *Phys. Fluids B* **5** (1993), pp. 590–596.

[30] S. Skupsky, R. W. Short, T. Kessler, R. S. Craxton, S. Letzring and J. M. Soures, "Improved laser-beam uniformity using the angular dispersion of frequency-modulated light", *J. Appl. Phys.* **66** (1989), no. 8, pp. 3456–3462.

[31] T. R. Boehly, V. N. Goncharov, O. Gotchev, et al., "Optical and plasma smoothing of laser imprinting in targets driven by lasers with SSD bandwidths up to 1 THz", *Phys. Plasmas* **8** (2001), no. 5, pp. 2331–2337.

[32] F. Walraet, G. Bonnaud and G. Riazuelo, "Velocities of speckles in a smoothed laser beam propagating in a plasma", *Phys. Plasmas* **8** (2001), no. 11, pp. 4717–4720.

[33] A. Fusaro, R. Collin, G. Riazuelo, P. Loiseau, O. Thauvin and D. Penninckx, "On the improvement of smoothing by spectral dispersion efficiency for laser-plasma interaction", *Phys. Plasmas* **31** (2024), no. 1, article no. 012110.

[34] J. Spurk and N. Aksel, *Fluid Mechanics*, 3rd edition, Springer, 2020.